# “Dynamics of a cavitating propeller in a water tunnel”

**by**

**S. Watanabe and C.E. Brennen**

**Originally published in 2003 in**
**ASME J. Fluids Eng., Vol. 125, No. 2, 283-292.**

**Satoshi Watanabe**
Associate Professor,
Department of Mechanical Engineering Science,
Kyushu University,
6-10-1 Hakozaki,
Higashi-ku, Fukuoka 812-8581, Japan
and
Visiting Associate,
Division of Applied Science and Engineering,
California Institute of Technology,
1200 E. California Boulevard,
Pasadena, CA 91125

**Christopher E. Brennen**
Division of Engineering and Applied Science,
California Institute of Technology,
Pasadena, CA 91125

# Dynamics of a Cavitating Propeller in a Water Tunnel

*This study investigates the unsteady dynamics and inherent instabilities of a cavitating propeller operating in a water tunnel. First, the steady characteristics of the cavitating propeller such as the thrust coefficient are obtained by applying continuity and momentum equations to a simple one-dimensional flow tube model. The effects of the tunnel walls as well as those of the propeller operating conditions (advance ratio and cavitation number) are explored. Then the transfer matrix of the cavitating propeller (considered to be the most appropriate way to describe the dynamics of propeller) is obtained by combining the simple stream tube model with the conventional cavity model using the quasi-static cavitation compliance and mass flow gain factor representation. Finally, the surge instability of a cavitating propeller observed by Duttweiler and Brennen (2001) is examined by coupling the present model of the cavitation with a dynamic model for the water tunnel. This analysis shows that the effect of tunnel walls is to promote the surge instability.*
[DOI: 10.1115/1.1524588]

## 1 Introduction

In devices such as pumps, turbines, and marine propellers, cavitation has many adverse effects including material erosion and performance degradation. In addition, it can give rise to instabilities that do not occur in single phase flow. For example, high-speed turbopumps often suffer from severe shaft vibrations due to cavitation instabilities such as cavitation surge and rotating cavitation. With ship's propellers, the fluctuating cavity volume due to the interaction between the propeller and the wake of ship hull can be a significant source of noise and even severe structural vibration of the ship. The large body of work on propeller-hull interactions has been summarized by Weitendorf [1].

Recently, a surge instability, which had not been previously reported, was observed by Duttweiler and Brennen [2] in their experimental work on a cavitating propeller operated in a water tunnel. The phenomenon seems to be similar to the well-known cavitation surge in pumps (Brennen [3]). This suggests that the dynamics of a cavitating propeller are system-dependent, whereas many investigators have implicitly assumed that propellers in water tunnels have dynamic characteristics similar to those operating in open conditions. In the past, studies of the cavitation dynamics of pumps developed the concept of a transfer matrix, which characterizes the relationship between the fluctuating pressure and mass flow rate at inlet and outlet (Brennen and Acosta [4]). In determining the elements of transfer matrix, two important parameters were introduced, namely the cavitation compliance and the mass flow gain factor. The cavitation compliance models the effective compressibility of a cavitating flow. The mass flow gain factor represents the response of the cavity volume to incoming mass flow rate variations. Later, this modeling of cavitating pumps led to the important conclusion that cavitation surge and rotating cavitation of pumps are caused by a positive mass flow gain factor (Brennen [5] and Tsujimoto et al. [6]). The above background suggests that it is useful to use the transfer matrix approach to describe the dynamics of a cavitating propeller in a water tunnel and to use this technique to explore the stability of these flows. In the present study, we construct a one-dimensional flow tube model that includes the effects of the tunnel walls as well as cavities on the propeller. First, we study the steady flow characteristics including the thrust force in order to examine the effects of tunnel walls. Then, the transfer matrix approach is used to model the dynamics of the cavitating propeller, and calculations are made for several cases with assumed cavitation characteristics. Finally, we examine the stability of these cavitating flows by coupling the propeller model with the dynamics of the water tunnel.

## 2 Outline of the One-dimensional Flow Tube Analysis

**2.1 Formulation of the Problem.** Consider the one-dimensional flow through a cavitating propeller in a water tunnel as shown in Fig. 1. The propeller (cross-sectional area $a_p$) is located on the centerline of the tunnel whose cross-sectional area is $A$. We consider a stream tube containing the propeller whose volumetric flow rate is denoted by $q$. For simplicity, it will be assumed that the flow is uniformly distributed across the propeller stream tube and is one-dimensional. Friction and mixing losses between the inner and outer flows are neglected. The low-frequency unsteady characteristics of the cavitating propeller will be analyzed under the assumption that the flow can be represented by a series of quasi-static states.

Referring to the propeller stream tube, the incoming and outgoing volumetric flow rates are different due to the rate of change of the cavity volume, $dV_c/dt$, where $V_c$ is the total cavity volume on the propeller blades. The continuity relation yields

$$u_1 a_1 - u_p^- a_p = -\int_{-\infty}^{0} \frac{\partial a}{\partial t} dx \tag{1}$$

$$u_2 a_2 - u_p^+ a_p = \int_{0}^{\infty} \frac{\partial a}{\partial t} dx \tag{2}$$

$$u_p^+ a_p - u_p^- a_p = dV_c/dt \tag{3}$$

$$u_2 a_2 + U_2(A - a_2) - u_1 A = dV_c/dt \tag{4}$$

where $u$ and $U$ denote velocities in the inner and outer flows, $a$ denotes cross-sectional area of the inner tube, and the subscripts 1, 2, and $p$, respectively, denote quantities far upstream, far downstream, and at the propeller. Superscripts $+$ and $-$, respectively, denote the outlet from and the inlet to the propeller. It has been assumed that the velocities in the inner and the outer flows are the same far upstream. The right-hand sides of Eqs. (1) and (2) represent the volume change of the stream tube upstream and downstream of the propeller; later these will be ignored for simplicity.

The relation between the pressures far upstream and far downstream is obtained by applying Bernoulli's equation in the outer flow as follows:

Contributed by the Fluids Engineering Division for publication in the JOURNAL OF FLUIDS ENGINEERING. Manuscript received by the Fluids Engineering Division February 1, 2002; revised manuscript received August 15, 2002. Associate Editor: S. L. Ceccio.

  

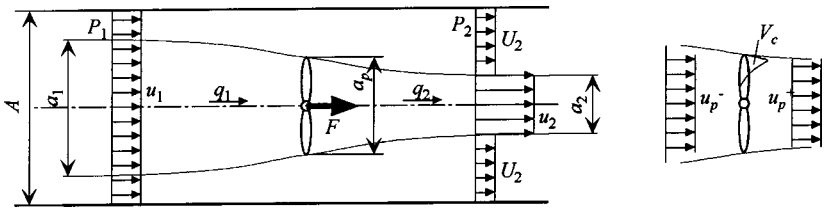


**Fig. 1 Propeller being operated at the center of axis**

$$P_2-P_1=\frac{1}{2}\rho(u_1^2-U_2^2)-\rho\int_{-\infty}^{\infty}\frac{\partial U}{\partial t}dx \tag{5}$$

where the last term of the right-hand side is the inertia effect in the control volume.

Now, we calculate the thrust force $F$ produced by the propeller in three ways. First, applying the momentum theorem to a control volume containing all the tunnel flow, we obtain

$$\rho u_1^2A+P_1A+F=\rho U_2^2(A-a_2)+\rho u_2^2a_2+P_2A+dM/dt.$$

The last term in the right-hand side is rate of the change of the momentum in the control volume, represented by

$$\begin{aligned}\frac{dM}{dt}&=\rho\frac{d}{dt}\int_{-\infty}^{\infty}[ua+U(A-a)]dx\\&=\rho\frac{d}{dt}\left\{\int_{-\infty}^{\infty}[ua+U(A-a)-u_1A]dx+\int_{-\infty}^{\infty}u_1Adx\right\}\\&=\rho\frac{d}{dt}\left\{\int_0^{\infty}\frac{dV_c}{dt}dx+A\int_{-\infty}^{\infty}u_1dx\right\}\\&=\rho\int_0^{\infty}\frac{d^2V_c}{dt^2}dx+\rho A\int_{-\infty}^{\infty}\frac{du_1}{dt}dx\end{aligned}$$

which yields

$$\begin{aligned}F=&\frac{1}{2}\rho(u_1-U_2)A(2u_2+U_2-u_1)+\rho(u_2+U_2)\frac{dV_c}{dt}\\&+\left[\rho A\int_{-\infty}^{\infty}\frac{\partial(u_1-U)}{\partial t}dx+\rho\int_0^{\infty}\frac{d^2V_c}{dt^2}dx\right].\end{aligned}\tag{6}$$

Second, we obtain the total pressure difference across the propeller from the Euler head,

$$\Delta p^T=\rho U_Tv_p=\rho U_T(U_T-u_p^+\cot\beta)-\rho\frac{c}{\sin\beta}\frac{du_p^+}{dt},$$

where $\beta$ and $c$, respectively, denote the discharge flow angle and the chord length of the blade. The last term in this equation represents the inertia effect of the fluid in the blade passage. Since the static pressure difference $p_{\text{out}}-p_{\text{in}}$ is given by

$$p_{\text{out}}-p_{\text{in}}=\frac{1}{2}\rho(U_T^2-u_p^{+2}\cot^2\beta)-\rho\frac{c}{\sin\beta}\frac{du_p^+}{dt}$$

and the thrust force can be computed as

$$\begin{aligned}F&=(p_{\text{out}}-p_{\text{in}})a_p+\rho(u_p^{+2}-u_p^{-2})a_p\\&=\frac{1}{2}\rho(U_T^2-u_p^{+2}\cot^2\beta)a_p+\rho(u_p^++u_p^-)\frac{dV_c}{dt}-\rho\frac{a_pc}{\sin\beta}\frac{du_p^+}{dt}.\end{aligned}\tag{7}$$

Third, the pressures $p_{\text{in}}$ and $p_{\text{out}}$ may be related to the upstream and downstream conditions using Bernoulli's equation:

$$p_{\text{in}}=P_1+\frac{1}{2}\rho u_1^2-\frac{1}{2}\rho u_p^{-2}-\rho\int_{-\infty}^{0}\frac{\partial u}{\partial t}dx$$

where the last term is the inertance in the stream tube. Applying Bernoulli's equation between the outlet of the propeller and far downstream, we obtain

$$\begin{aligned}p_{\text{out}}&=P_2+\frac{1}{2}\rho\left(u_2^2+v_p^{+2}\frac{a_p}{a_2}\right)-\frac{1}{2}\rho(u_p^{+2}+v_p^{+2})+\rho\int_0^{\infty}\frac{\partial u}{\partial t}dx\\&=P_2+\frac{1}{2}\rho u_2^2-\frac{1}{2}\rho u_p^{+2}+\frac{1}{2}\rho(U_T-u_p^+\cot\beta)^2\left(\frac{a_p}{a_2}-1\right)\\&\quad+\rho\int_0^{\infty}\frac{\partial u}{\partial t}dx.\end{aligned}$$

Then the thrust force $F$ follows as

$$\begin{aligned}F&=(p_{\text{out}}-p_{\text{in}})a_p+\rho(u_p^{+2}-u_p^{-2})a_p\\&=\frac{1}{2}\rho\left[(u_2^2-U_2^2)+(U_T-u_p^+\cot\beta)^2\left(\frac{a_p}{a_2}-1\right)\right]a_p\\&\quad-\frac{1}{2}\rho(u_p^++u_p^-)\frac{dV_c}{dt}+\rho a_p\int_{-\infty}^{\infty}\frac{\partial(u-U)}{\partial t}dx.\end{aligned}\tag{8}$$

For the purpose of the general discussion, we have considered all possible unsteady effects in the above formulation, namely the effects of volume change of the stream tubes in Eqs. (1) and (2), the inertia effects upstream and downstream of the propeller in Eqs. (5), (6), and (8), and the inertia effect in the propeller in Eq. (7) as well as the effects of the cavity volume change $dV_c/dt$ in Eqs. (3) and (4). To evaluate many of these terms, we need to know the shape of the stream tube, which is beyond the scope of the present one-dimensional stream tube analysis. Consequently, some compromises are needed in order to proceed. First we neglect the stream tube volume changes in Eqs. (1) and (2) on the basis that these cancel and thus produce no net perturbation within the water tunnel. We note, however, that this superficial argument may need further examination. Second, we neglect the inertance terms in Eqs. (5), (6), and (8) on the basis that past experience has suggested that we can consider these contributions to be lumped into the other inertance contributions in the tunnel circuit. Again this may need additional examination in the future. In summary, we choose to examine only the unsteady effects associated with $dV_c/dt$ in Eqs. (3) and (4).

Summarizing, we note that the eight equations (1) through (8) contain eight unknowns $U_2$, $u_2$, $u_p^+$, $u_p^-$, $a_1$, $a_2$, $F$, and $P_2$ assuming that the propeller operating parameters $u_1$, $P_1$, $u_T$, the discharge flow angle, $\beta$, and the rate of change of the cavity volume, $dV_c/dt$, are given. Information on the discharge flow angle $\beta$ especially for cavitating conditions will be discussed in the following subsection. The rate of change of the cavity volume, $dV_c/dt$, will be modeled in Section 2.3.

**2.2 Discharge Flow Angle.** To quantify the discharge flow angle $\beta$, we resort to an empirical model for the deviation angle, $\theta$

(the difference between the discharge blade angle $\beta_2$ and the discharge flow angle $\beta$), which takes into account the fact that the deviation will be increased by the presence of cavities on the propeller blades. Specifically, we adopt the following empirical model for the deviation angle:

$$\theta = 0 \qquad \text{for } \lambda > \lambda_{cr}$$

$$\theta = \left(\beta_2 - \tan^{-1}\frac{u_p}{U_T}\right)\left(1 - \frac{\lambda}{\lambda_{cr}}\right)^2 \quad \text{for } \lambda > \lambda_{cr} \tag{9}$$

where we have introduced the parameter $\lambda = \sigma/2\alpha$, where $\sigma = 2(p_{\text{in}} - p_v)/\rho U_T^2$ is the operating cavitation number of the propeller and $\alpha = \beta_1 - \tan^{-1}(u_p/u_T)$ is the incidence angle on the propeller blades. The argument for this single parameter representation, $\theta(\lambda)$, is that classical linear theory (Tulin [7] and Brennen [8]) shows that the cavity length to chord ratio is a function only of $\lambda$ and consequently the expected deviation should similarly be a function of $\lambda$. Though nonlinear and three-dimensional effects may generate departures from this simple functional dependence, it seems appropriate to proceed with this simplification in this approximate analysis.

Equation (9) has the properties that, if the cavity is small ($\lambda$ is large), the flow discharges from the propeller parallel to the blade. At the other extreme, when the cavity is very long ($\lambda \to 0$), the propeller performance will be degraded and the flow turning angle through the propeller diminished (there may be a certain small $\lambda$ at which the propeller breaks down but this detail is neglected for simplicity.) The critical value, $\lambda_{cr}$, below which the deviation begins, could be determined theoretically or empirically. This study will use a typical value of $\lambda_{cr} = 1$.

**2.3 Cavity Volume Change.** We assume that the cavity volume $V_c(p_{\text{in}}, u_p^-)$ is a function of the inlet pressure $p_{\text{in}}$ and inflow velocity $u_p^-$. Then, the rate of change of the cavity volume can be expressed as

$$\frac{dV_c}{dt} = -K\frac{dp_{\text{in}}}{dt} - M\frac{du_p^-}{dt} \tag{10}$$

where $K = -\partial V_c/\partial p_{\text{in}}$ and $M = -\partial V_c/\partial u_p^-$ are, respectively, the cavitation compliance and the mass flow gain factor (Brennen and Acosta [4]). These important parameters are nondimensionalized as follows:

$$\frac{K^*}{2\pi} = -\frac{\partial V_c/a_p R}{\partial \sigma} = -\frac{\rho U_T^2/2}{a_p R}\frac{\partial V_c}{\partial p_{\text{in}}} = \frac{\rho R^2 \Omega^2}{2\pi R^3}K = \frac{1}{2\pi}\frac{\rho \Omega^2}{R}K$$

$$M^* = -\frac{\partial V_c/a_p R}{\partial u_p^-/U_T} = -\frac{U_T}{a_p R}\frac{\partial V_c}{\partial u_p^-} = \frac{R\Omega}{\pi R^3}M = \frac{\Omega}{\pi R^2}M$$

where $\Omega$ is the rotational frequency of the propeller, and $K^*$ and $M^*$ are nondimensional values of the cavitation compliance and the mass flow gain factor used by Duttweiler and Brennen [2]. In this study, the values of $K$ and $M$ are estimated using free streamline theory (Otsuka et al. [9] and Watanabe et al. [10]).

## 3 Steady Calculation

In this section, we discuss the steady flow solutions of Eqs. (1) to (8) by eliminating the unsteady terms. Then, Eqs. (1)–(10) can be solved provided the operating conditions $u_1$, $P_1$, $U_T$ and the discharge flow angle, $\beta$, are specified. For the purposes of illustration, we choose to present results for typical blade angles, $\beta_1$ and $\beta_2$, of 25 deg. Moreover, the results are best presented using the following nondimensional parameters; the advance ratio $J_1$, a propeller flow coefficient $J_p$ and a thrust coefficient of the propeller $C_T$ defined as follows:

$$J_1 = \pi u_1/U_T$$

$$J_p = \pi\phi = \pi u_p/U_T$$

$$C_T = F/\tfrac{1}{2}\rho U_T^2 a_p$$

where $\phi$ is the propeller flow coefficient (also used in describing pump flows). As shown later, if we decrease the incoming velocity $u_1$, the inner flow tube expands far upstream and its cross-sectional area $a_1$ reaches that of the tunnel, $A$, at a certain value of $u_1$. When the incoming velocity is smaller than this value, Eq. (5) no longer applies. In such cases, the steady solution is obtained by setting $a_1 = A$ and $U_2 = 0$, and eliminating Eq. (4), because it becomes identical to the combination of Eqs. (1)–(3).

**3.1 Noncavitating Results.** Results for the noncavitating case (no deviation angle) are shown in Fig. 2. Various values of the cross-sectional area ratio, $A/a_p$, were selected in order to examine the effect of the presence of the tunnel walls. The case with $A/a_p = 1$ corresponds closely to that of a typical axial flow pump, because all the flow from upstream proceeds through the propeller (assuming no tip leakage flow for simplicity) and there is no outer flow. For the cases with $A/a_p = 2$ and 10, a critical advance ratio (approximately 0.58 and 0.12 for $A/a_p = 2$ and 10, respectively) exists at which the cross-sectional area of stream tube far upstream $a_1$ equals to that of the duct $A$. Below the critical advance ratio, the propeller works like an axial flow pump with all fluid flowing through the propeller. The results for $A/a_p = 10$ have been found to adequately represent the open condition ($A/a_p = \infty$) except at very low advance ratios, where the analysis breaks down for reasons discussed elsewhere.

Figures 2(*a*)–(*c*) present the thrust coefficient $C_T$, the propeller flow coefficient $J_p$, and the cross-sectional areas $a_1/a_p$ and $a_2/a_p$ plotted against the advance ratio $J_1$. For $A/a_p = 2$ and 10, as the advance ratio decreases, the flow coefficient decreases gradually and the thrust coefficient increases gradually. This is because, as the advance ratio is decreased, the propeller is taking fluid from a wider upstream stream tube. The variations of the thrust coefficient and the flow coefficient are more gradual than those for $A/a_p = 1$. However, below the critical advance ratio where the propeller works like an axial flow pump, the flow coefficient rapidly decreases and the thrust coefficient rapidly increases, and these variations are more significant than for $A/a_p = 1$. The decrease in the flow coefficient is related directly to the advance ratio, so that the slope of the flow coefficient in Fig. 2(c) gets steeper as the duct gets wider.

Given these steady operating characteristics, it is valuable to consider the quasi-static response to low frequency fluctuations of the incoming flow velocity $u_1$. For illustrative purposes, we compare the case of $A/a_p = 2$ with that for a pump ($A/a_p = 1$). Consider first the case when the advance ratio is larger than the critical advance ratio. As the upstream flow velocity varies, the flow rate through the propeller varies less when $A/a_p = 2$ than when $A/a_p = 1$ (Fig. 2(b)). However, when the advance ratio is smaller than the critical value, this trend is reversed. If the propeller were cavitating, these results would suggest that, at larger advance ratios, the mass flow gain factor will be smaller for $A/a_p = 2$ than that for $A/a_p = 1$, whereas at smaller advance ratios, the mass flow gain factor will be larger for $A/a_p = 2$. This is important since the mass flow gain factor is responsible for cavitation instabilities of turbomachinery and a large mass flow gain factor implies a more unstable system.

The surge instability of a cavitating propeller, reported by Duttweiler and Brennen [2], is an example of cavitation instability caused by a positive mass flow gain factor. They examined two different configurations of the propeller, one in which the propeller is operated in front of a support fairing, and the other in which the propeller is operated downstream of that fairing, and observed a violent surge instability only for the latter case. The explanation for this difference is unknown, but one explanation might be as follows. The presence of the fairing can be considered to be the blockage, so that the effective flow path upstream of the propeller is smaller for the case with the propeller operated downstream of

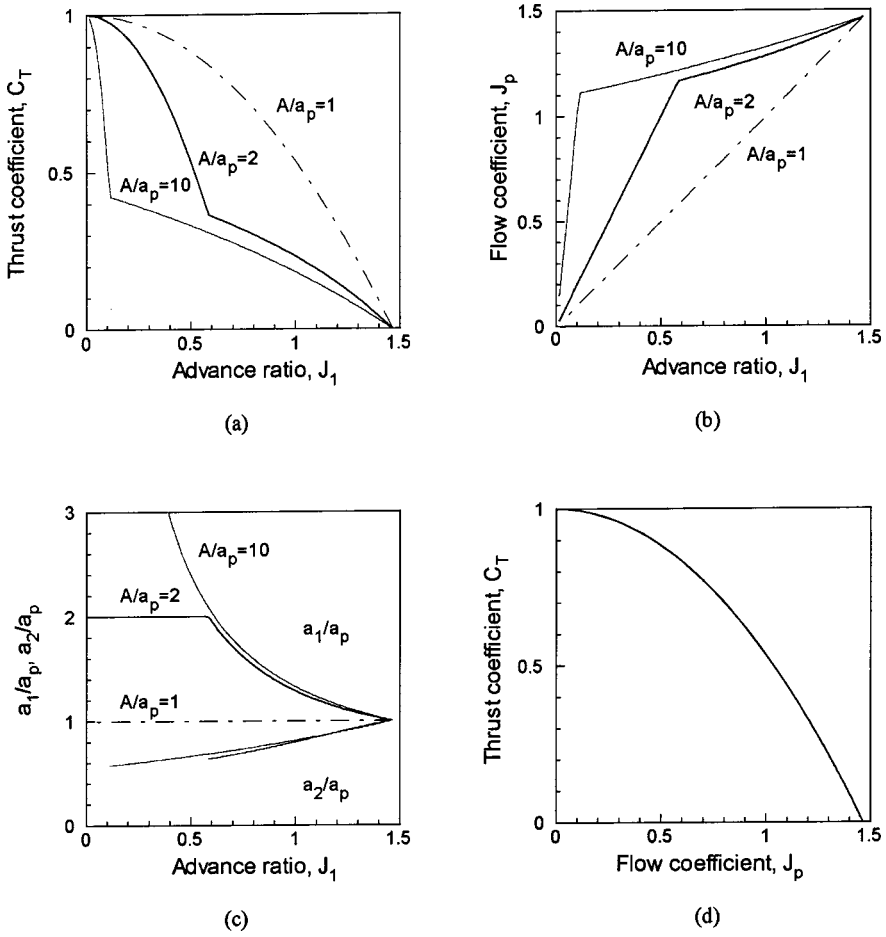


**Fig. 2 Steady characteristics of noncavitating propeller with the constant exit flow angle of $\beta=25$ deg. The propeller is located at the center of the duct with cross-sectional areas of $A/a_p=1$, 2, and 10.**

the fairing. Figure 2(b) indicates that the critical value of the advance ratio is larger when the propeller is operated in the narrower duct. So, as the advance ratio decreases, the propeller could readily shift into operation as a pump. The result would be that the mass flow gain factor is larger for the propeller operated downstream of the fairing.

**3.2 The Case With Cavitation.** Figures 3(a) and (b) present the thrust coefficient $C_T$ and the flow coefficient $J_p$ plotted against the advance ratio $J_1$ for various cavitation numbers, $\sigma$. Recall that in this model the presence of the cavitation affects the results only by altering the exit flow angle (Eq. (9)). Figure 4 shows the thrust coefficient $C_T$ plotted against the cavitation num-

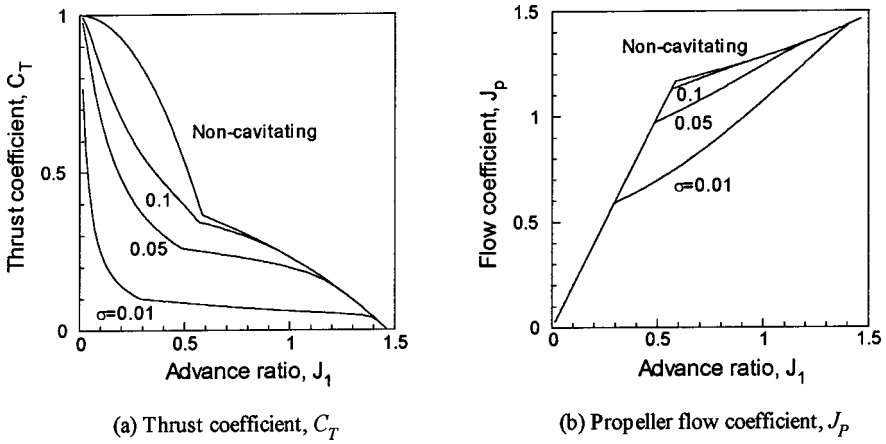


**Fig. 3 Effect of cavitation number on thrust coefficient $C_T$ and propeller flow coefficient $Jp$. The presence of cavitation is taken into account through the deviation angle of the flow exiting from the propeller [$A/a_p=2$].**

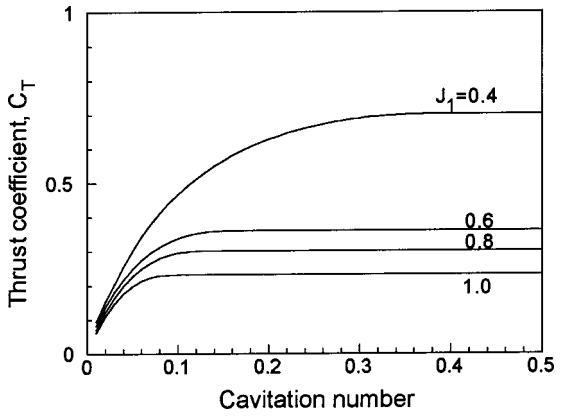


**Fig. 4 Thrust coefficient $C_T$ versus cavitation number $\sigma$ for various advance ratios $J_1$. The effects of cavitation are taken into account through the deviation angle of the exit flow.**

ber $\sigma$ for various advance ratios $J_1$. Note that the deterioration of the thrust coefficient as a result of cavitation is well simulated by introducing the deviation angle due to the presence of cavitation modeled by Eq. (9).

Note also that the flow coefficient has a steeper slope against the advance ratio for smaller cavitation numbers as shown in Fig. 3(*b*). This is because, as the cavitation number is decreased, the thrust coefficient decreases because of the losses through the deviation angle associated with the presence of cavitation on the propeller blades. Then the flow rate through the propeller must decrease to compensate for the decreased thrust. The steeper slope of the flow coefficient against the advance ratio means that the flow rate through the propeller is more sensitive to the upstream flow variation and the mass flow gain factor is larger because a small advance ratio change makes a large propeller flow rate change. This will tend to promote a surge instability.

## 4 Quasi-Steady Analysis

In this section, we analyze the low-frequency unsteady characteristics of the cavitating propeller. The system of equations consists of nonlinear equations. However, in order to utilize the conventional transfer function methodology, we linearize the problem. For example, the upstream flow velocity is expressed by

$$u_1=\overline{u_1}+\mathrm{Re}[\tilde{u}_1\exp(j\omega t)].$$

After substituting similar expressions for all the unknowns, Eqs. (1)–(8) are then divided into steady and unsteady parts and linearized under the assumption of small fluctuations. The unsteady parts of the equations consist of linear equations for the unsteady components, the eight unknowns $U_2$, $u_2$, $u_p^+$, $u_p^-$, $a_1$, $a_2$, $F$, and $P_2$ as well as the quantities, $u_1$, $P_1$, $\beta$, and $dV_c/dt$. The unsteady component of $\beta$ is obtained by the linearized version of Eq. (9), which diminishes for larger values of $\sigma$. The rate of the change of cavity volume $dV_c/dt$ is given by Eq. (10).

The total mass flow rate and static pressure downst ream of the propeller are defined downstream of the mixing of the flows in the inner and outer stream tubes. The mass flow rate and pressure after the mixing, $m_2$ and $P_2'$, are obtained by applying continuity and momentum conservation as follows:

$$m_2=\rho[u_2a_2+U_2(A-a_2)]=\rho u_2'A$$

$$P_2A+\rho u_2^2a_2+\rho U_2^2(A-a_2)=P_2'A+\rho u_2'^2A.$$

Using these equations, we can relate the downstream fluctuations to the inlet fluctuations using the conventional transfer matrix (Brennen [3]):

$$\begin{Bmatrix}\tilde{p}_2^T\\ \tilde{m}_2\end{Bmatrix}=\begin{bmatrix}T_{11} & T_{12}\\ T_{21} & T_{22}\end{bmatrix}\begin{Bmatrix}\tilde{p}_1^T\\ \tilde{m}_1\end{Bmatrix}$$

where $p^T$ and $m$ are total pressure and mass flow rate, respectively.

**4.1 Example Calculations.** Figure 5 presents a typical calculation of the transfer matrix for an advance ratio of $J_1=1.0$ and duct cross-sectional areas of $A/a_p=1$, 2 and 10. For illustrative purposes, values of the compliance and mass flow gain factor $(K^*/2\pi,M^*)$ of (0.1,1.0) are selected since these values are typical of those obtained by previous researchers, [3–5]. The change of the exit flow angle $\beta$ is neglected for simplicity, assuming $\sigma=\infty$. Note that $T_{21}$ takes a similar value for all cases while there are large differences in the other elements of transfer matrix. If we consider the case with no discharge mass flow fluctuations, the

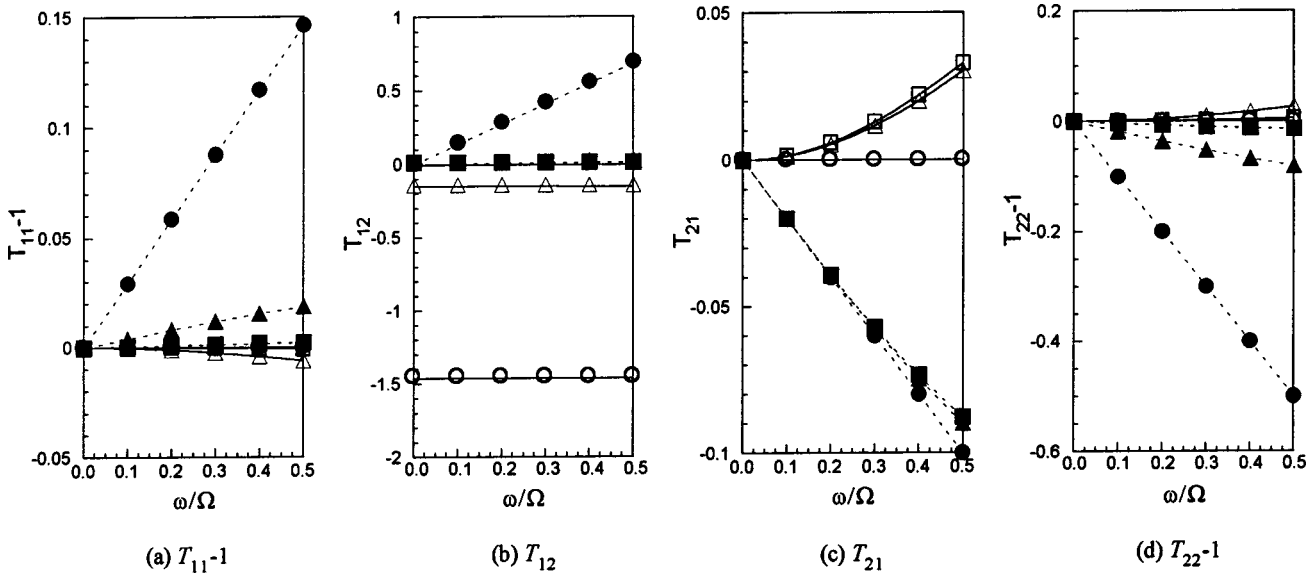


**Fig. 5 Calculated transfer matrices of the cavitating propeller for an advance ratio, $J_1=1.0$, and $(K^*/2\pi,M^*)=(0.1,1.0)$ and for various values of $A/a_p=1$(○ ●), 2(△ ▲), and 10(□ ■), where open and closed symbols denote real and imaginary parts of matrix elements, respectively. The change of the exit flow angle of $\beta$ is neglected.**

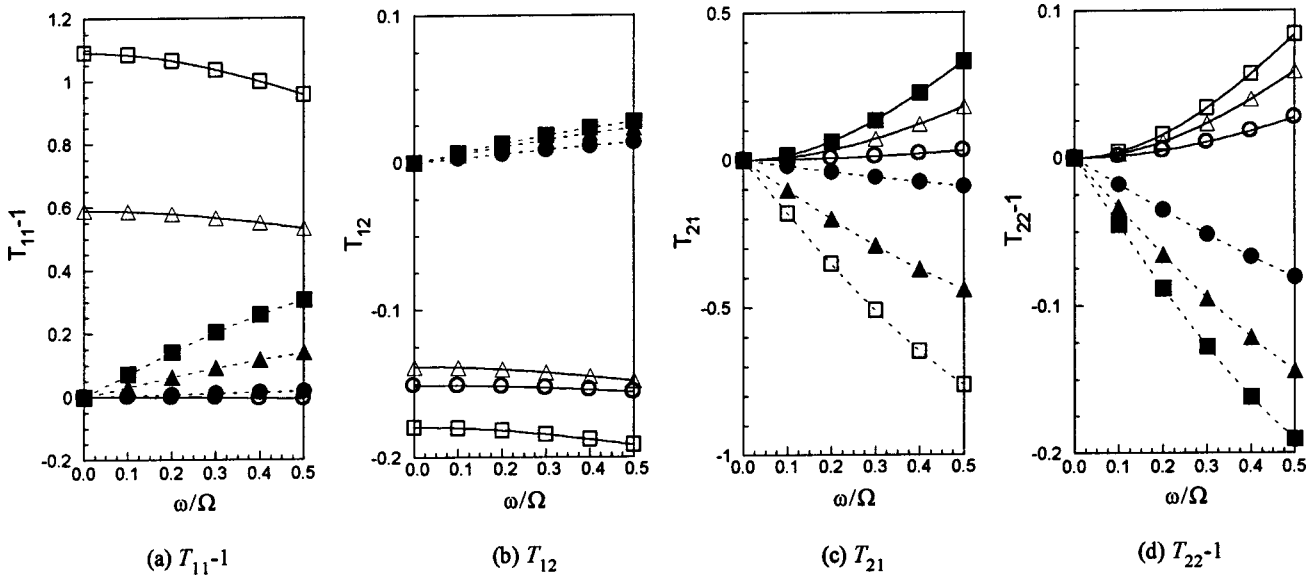


**Fig. 6 Calculated transfer matrices of the cavitating propeller with $A/a_p=2$ and an advance ratio, $J_1=1.0$, for the various cavitation numbers $\sigma=\infty$(○ ●), 0.05(△ ▲), and 0.01(□ ■), where open and closed symbols denote real and imaginary parts of matrix elements, respectively**

propeller operated in a wider duct (for example $A/a_p=10$) might be the most stable because of the large negative impedance with the small imaginary part of $T_{22}$ and the large imaginary part of $T_{21}$.

Figure 6 shows the transfer matrix for an advance ratio of $J_1=1.0$, a duct cross-sectional area of $A/a_p=2$ and various cavitation numbers. The values of $(K^*/2\pi,M^*)$ are again set to be (0.1,1.0) for all cases. Head deterioration due to the presence of cavitation is implicitly included through the assumed changes in the deviation angle $\beta$. All elements are affected by the head deterioration, but the stability does not seem to be significantly changed. The imaginary parts of both $T_{21}$ and $T_{22}$ are increased by the head deterioration.

**4.2 Coupling With Streamline Theory.** Otsuka et al. [9] and Watanabe et al. [10] have obtained the cavitation compliance and mass flow gain factor of cavitating cascades by a free streamline theory. Here, we utilize their results in order to assess appropriately values of $K^*/2\pi$ and $M^*$. The values of $(K^*/2\pi,M^*)$ obtained by those investigations are shown in Fig. 7 for typical values for the solidity (1.0), the stagger angle ($\beta=25.0$ deg) and the number of blades ($Z_N=5$). Because Otsuka et al. and Watanabe et al. examine only two-dimensional flows around foils, the cavity size per blade is treated as a cross-sectional area $V_{cpb}$ (not a volume) and the scaling as $V_c=Z_NRV_{cpb}/2$ is used as a best estimate. Note that $(K^*/2\pi,M^*)$ are functions of the parameter $\lambda=\sigma/2\alpha$, where $\sigma$ is cavitation number at inlet to the propeller.

Now, rather than use the fixed values of $K^*$ and $M^*$, we calculate the transfer function using the above relations between $(K^*/2\pi,M^*)$ and $\lambda=\sigma/2\alpha$. Results are shown in Figs. 8 and 9 for $A/a_p=2$ and 10, respectively. Three cases with different upstream cavitation numbers $\sigma_{up}=0.15$, 0.20, and 0.5 are examined. The advance ratio $J_1$ is 1.0, which is larger than the critical value. Note that, only for the case with $\sigma_{up}=0.15$, is the parameter $\lambda=\sigma/2\alpha$ less than unity and therefore only in this case is there head deterioration with increasing deviation angle. The cavitation compliance $K^*/2\pi$ varies from 0.018 to 0.172 for $A/a_p=2$ and from

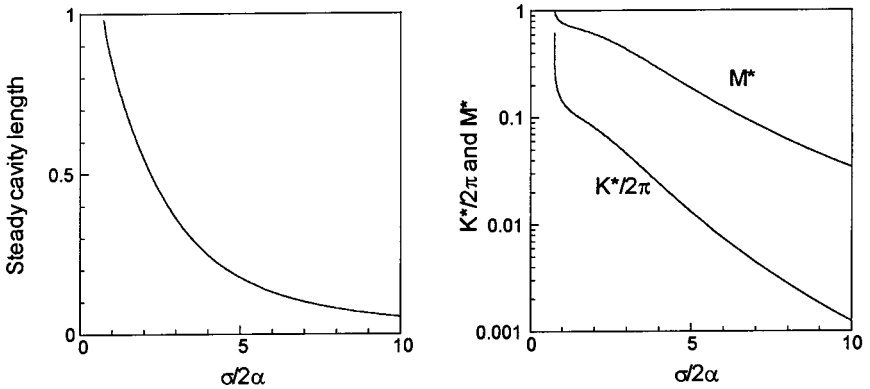


**Fig. 7 Steady cavity length and the quasi-static cavitation compliance and mass flow gain factor plotted against $\sigma/2\alpha$ obtained by a free streamline theory (Watanabe et al. [10]). [solidity=1.0, stagger angle $\beta=25.0$ deg, $Z_N=5$].**

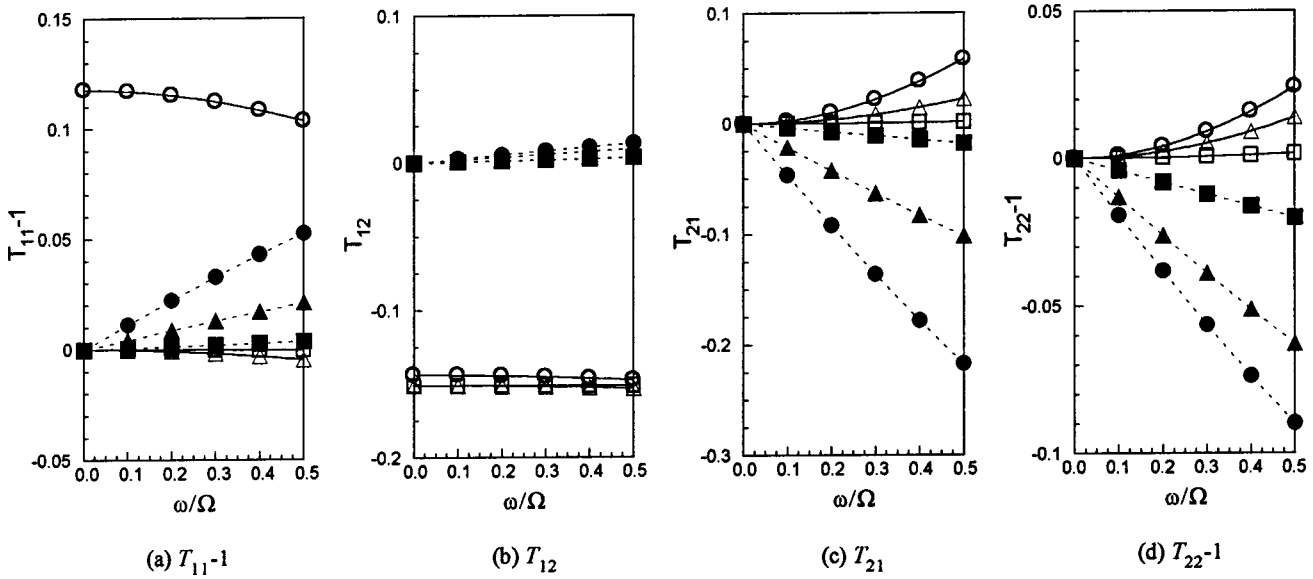


**Fig. 8 Calculated transfer matrices of the cavitating propeller with $A/a_p=2$ and an advance ratio, $J_1=1.0$, for the various cavitation numbers $\sigma_{up}=0.15$(○ ●), 0.20(△ ▲), and 0.50(□ ■), where open and closed symbols denote real and imaginary parts of matrix elements, respectively. The values of cavitation compliance and mass flow gain factor are obtained from Fig. 7.**

0.009 to 0.143 for $A/a_p=10$. The mass flow gain factor $M^*$ varies from 0.231 to 0.831 for $A/a_p=2$ and from 0.140 to 0.777 for $A/a_p=10$. These values are slightly smaller for the case with $A/a_p=10$. This is because, as shown in Fig. 2($b$), the flow coefficient is slightly larger for the case with $A/a_p=10$, and this results in a smaller incidence angle.

From Figs. 8 and 9, it is seen that $T_{21}$ takes similar values for all the cavitation numbers, while the other elements of the transfer matrix are much affected by the presence of cavitation. Note that the elements $T_{11}-1$, $T_{12}$ and $T_{22}-1$ are much smaller for the case with $A/a_p=10$, whereas the element $T_{21}$ is the same order for both cases. This implies that the propeller with $A/a_p=10$ is more stable since the imaginary part of $T_{22}$ is smaller; in other words the effective mass flow gain factor is smaller.

The advance ratio $J_1$ is also an important parameter, because there is a critical value which separates normal operation from pump-like operation. It would be interesting to compare the transfer matrices for normal and pump-like operations, but unfortunately the free streamline theory is only applicable to high flow rates and high advance ratios.

**4.3 Facility and Cavitation Dynamics.** We now consider the dynamics of the whole system of the water tunnel, taking the experimental arrangement used by Duttweiler and Brennen [2] as an example. Figure 10 shows the schematic of the facility and cavitation dynamics used by Duttweiler and Brennen. The facility dynamics are characterized by (i) the compliance, $C_{ot}[=405]$, of the overflow tank that allows control of the pressure within the

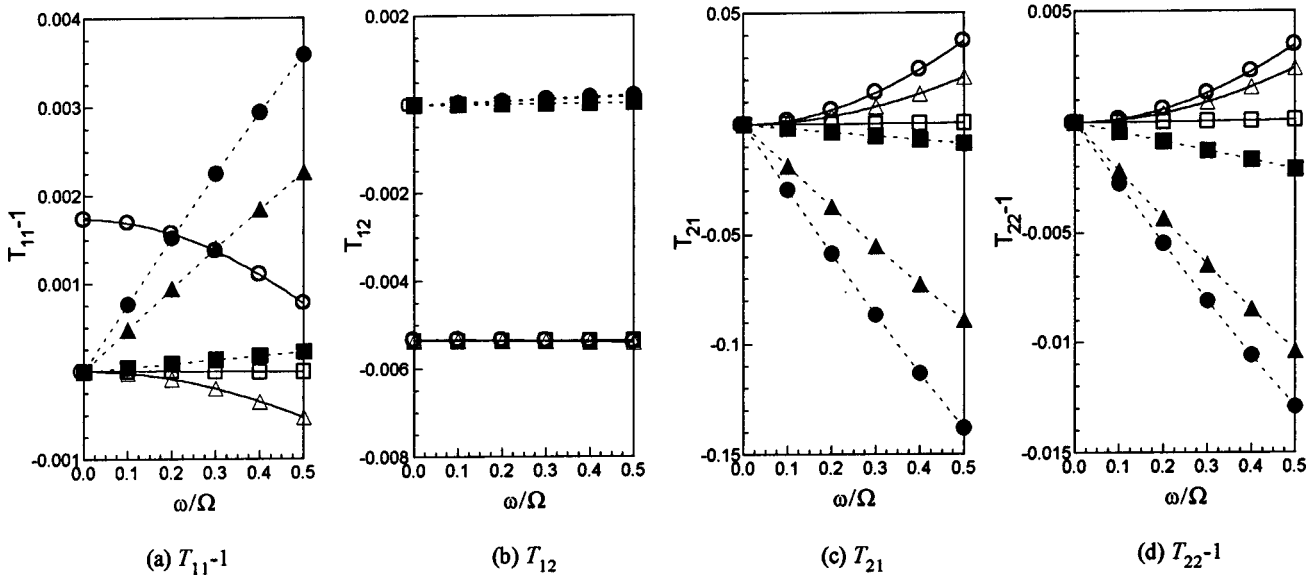


**Fig. 9 Calculated transfer matrices of the cavitating propeller with $A/a_p=10$ and an advance ratio, $J_1=1.0$, for the various cavitation numbers $\sigma_{up}=0.15$(○ ●), 0.20(△ ▲), and 0.50(□ ■), where open and closed symbols denote real and imaginary parts of matrix elements, respectively. The values of cavitation compliance and mass flow gain factor are obtained from Fig. 7.**

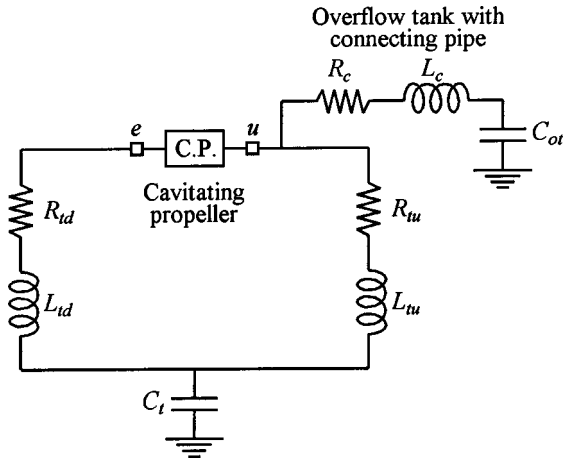


**Fig. 10 Schematic of facility and cavitation dynamics**

facility and therefore has the only deliberate free surface, (ii) the resistance, $R_c[=0.0295]$, and inertance, $L_c[=57.3]$, of the pipe connecting the tunnel with the overflow tank, (iii) the compliance, $C_t[=1970]$, associated with the expansion and contraction of the walls of the tunnel, and (iv) the resistances, $R_{tu}[=0.0]$ and $R_{td}[=0.0]$, and inertances, $L_{tu}[=0.953]$ and $L_{td}[=2.10]$, associated with the typical flow paths upstream and downstream of the cavitating propeller. The parameters used by Duttweiler and Brennen [2] were normalized using the propeller radius, $R$, and the propeller rotation frequency, $\Omega$, to obtain the values shown in the square brackets after each symbol.

The dynamics of the system can be characterized by considering the response of the system to a fluctuating mass flow rate, $\tilde{m}_e$, injected at some specific location, $e$, in the system (Fig. 10). We define a system impedance, $Z$, as follows:

$$Z=\frac{\tilde{p}_e^T}{\tilde{m}_e}$$

where $\tilde{p}_e^T$ is the total pressure fluctuation at $e$. Note that, in general, the impedance $Z$ is complex.

Using the present methodology coupled with the dynamics of the water tunnel identified by Duttweiler and Brennen [2], we have calculated the system impedance $Z$ for the case with advance ratio $J_1=0.64$ and cavitation number $\sigma_{up}=0.25$. The real part of $Z$ is plotted in Fig. 11 against the normalized frequency, $\omega/\Omega$. In calculating the transfer matrix of propeller, we set $A/a_p=3.16$ and $Z_N=6$ and the cavitation characteristics $(M,K)$ shown in Fig. 7 were used. The positive peak at $\omega/\Omega=0.007$ is largely due to the impedance of overflow tank. The shallow negative peak around

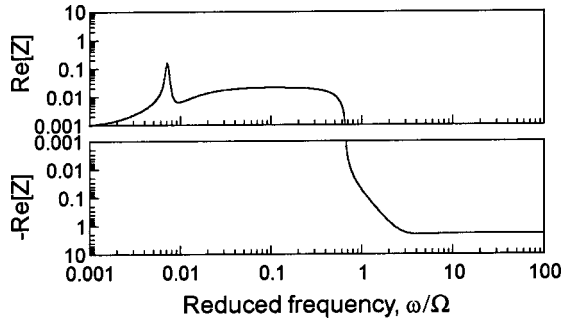


**Fig. 11 Example of the system impedance, *Z*. Mass flow fluctuation is imposed at point *e* in Fig. 10. Real part of the system impedance is plotted against the various excited frequencies. [$J_1=0.64$, $\sigma_{up}=0.25$. *K** and *M** are evaluated from Fig. 7.]**

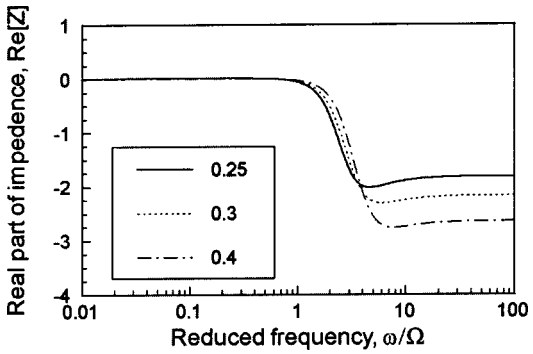


**Fig. 12 Real part of the system impedance for various upstream cavitation numbers, $\sigma_{up}$. [$J_1=0.64$. *K** and *M** are evaluated from Fig. 7.]**

$\omega/\Omega=3$ might indicate the existence of surge instability, but the frequency is much higher than the value of $\omega/\Omega=0.2$ observed in the experiments of Duttweiler and Brennen [2]. Moreover, if we compare the present result with the system impedance obtained by Duttweiler and Brennen, we find that the frequency obtained by the present analysis is still much higher than the experimental values and the peak is much shallower. The explanation for this discrepancy is unknown, but the following may be pertinent. In the pump cases, the elements $T_{21}$ and $T_{22}-1$ are purely imaginary when the cavitation compliance and mass flow gain factor considered are purely real. On the other hand, in the propeller cases, $T_{21}$ and $T_{22}-1$ are complex because of our one-dimensional flow tube model. Complex values of $T_{21}$ and $T_{22}-1$ mean that the system responds as if we have complex values of the cavitation compliance and mass flow gain factor.

Figure 12 shows the real part of system impedance for the case with three different cavitation numbers $\sigma_{up}=0.25$, 0.2, and 0.15. The frequency at the negative peak decreases as the cavitation number is decreased, but is still larger than the experimental value of $\omega/\Omega=0.2$. One possible explanation for the discrepancy is that the model considers only the sheet cavitation on the blade surface. However, a large volume change in the tip cavity during a surge cycle was clearly observed in experiments by Duttweiler and Brennen [2]. It is important to note that the present one-dimensional stream tube model may lose validity at the lower advance ratios, where the flow around the propeller is very three-dimensional. However, because the surge instability is a system instability in which the large amount of fluid is accelerated one-dimensionally by the volume change of cavities, the present method is expected to be applicable even at those low advance ratios provided we could evaluate the cavitation compliance and the mass flow gain factor of all the cavitation including the tip vortex cavities. The unsteady characteristics of tip vortex cavities need further investigation.

Figure 13 shows the values of $\sigma/2\alpha$ just upstream of the propeller plotted in the $\sigma_{up}-J_1$ plane obtained by the present steady analysis. According to the linear theory [11], cavitation instabilities of a two-dimensional cascade are dependent only on the parameter $\sigma/2\alpha$. The instability boundary obtained by Duttweiler and Brennen [2] is also plotted in the figure. We can see that the value of $\sigma/2\alpha$ is nearly constant along the instability boundary, which means that the stability depends on the local condition at the propeller inlet rather than the advance ratio or upstream cavitation number.

## 5 Conclusion

This paper has evaluated the quasi-static transfer matrices for a cavitating propeller operating in a water tunnel. Simple flow models based on a one-dimensional flow tube analysis are used. The effects of the presence of cavitation, and of the blockage due to

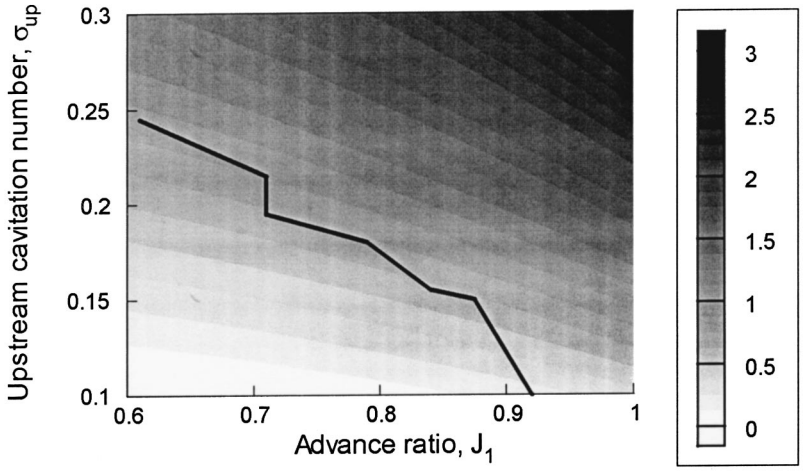


**Fig. 13 The ratio of cavitation number to twice of incidence angle, $\sigma/2\alpha$, is plotted for various upstream conditions $\sigma_{up}$ and $J_1$. The solid line represents the boundary of the onset of surge instability observed by Duttweiler and Brennen [2], showing that the surge instability occurs in the region below this line.**

the tunnel walls are examined. The former is modeled by the head deterioration through the deviation of the exit flow, and the conventional cavitation characteristics, the cavitation compliance and the mass flow gain factor. These characteristics are estimated by a free streamline theory.

It is found that the presence of the tunnel wall has a large effect on the stability of propeller operation. In an open condition, the flow rate through the propeller is not very sensitive to the advance ratio. However, in the presence of the tunnel walls, the propeller flow rate changes much more in response to the advance ratio change. This implies that, if there are flow rate fluctuations, the flow rate through the propeller varies more when there are tunnel walls and this may result in unstable operation of the propeller. When the advance ratio is the same, the flow rate through the propeller is smaller and the incidence angle is larger if the propeller is operated in a tunnel with a smaller cross-sectional area. Large incidence angles can result in the flow instabilities and enhance the occurrence of cavitation. Transfer matrices for the cavitating propeller are evaluated by assuming the flow is quasi-static. The transfer matrices show that the propeller operating in the narrower tunnel is much more unstable. If the propeller is operated in a wider tunnel or in an open condition, the effects of a mass flow gain factor are reduced because the variation of the propeller flow rate is smaller even when the total flow rate changes substantially.

Finally, we have tried to obtain the frequency of surge instability from the system impedance, but failed. One of the possible explanations for the discrepancy is that the model considers only sheet cavitation on the blade surface. A large volume change in the tip cavity during a surge cycle was also observed in experiments and may well contribute to the discrepancy.

## Nomenclature

$A$ = cross-sectional area of water tunnel
$a$ = cross-sectional area of inner stream tube
$C_{ot}$, $C_t$ = compliance of overflow tank and water tunnel
$C_T$ = thrust coefficient
$c$ = chord length
$F$ = thrust force of propeller
$J_1$, $J_p$ = advance ratio and flow coefficient
$K^*$ = cavitation compliance
$L_c$ = innertance of the connecting duct between water tunnel and overflow tank
$L_{tu}$, $L_{td}$ = innertance of the duct upstream and downstream of the tunnel
$M^*$ = mass flow gain factor
$m$ = mass flow rate
$P_1$, $P_2$ = static pressure far upstream and downstream
$p_{\text{in}}$ and $p_{\text{out}}$ = static pressure at inlet and outlet of propeller
$p^T$ = total pressure
$p_v$ = vapor pressure
$q$ = volumetric flow rate of the stream tube
$R$ = propeller radius
$R_c$ = resistance of the connecting duct between water tunnel and overflow tank
$R_{tu}$, $R_{td}$ = resistance of the duct upstream and downstream of the tunnel
$U$ = axial velocity in the outer stream tube
$U_T$ = rotational velocity of propeller
$u$ = axial velocity component in inner stream tube
$T_{ij}$ = elements of transfer matrix
$V_c$ = cavity volume on the propeller blade
$v$ = tangential velocity component in inner stream tube
$Z$ = system impedance
$\alpha$ = incidence angle
$\beta$ = discharge flow angle
$\beta_1$, $\beta_2$ = inlet and outlet blade angles of propeller
$\lambda$ = parameter defined by $\sigma/2\alpha$
$\sigma$, $\sigma_{\text{up}}$ = cavitation numbers at propeller inlet and far upstream
$\Omega$ = rotational frequency of propeller
$\omega$ = angular frequency of fluctuations

### Superscripts

$\bar{}$ = steady (mean) components of variables
$\sim$ = unsteady components of variables
$+$, $-$ = variables just upstream and downstream of propeller

### Subscripts

1,2 = far upstream and downstream
e = at the point of excitation in the system shown in Fig. 10
p = at the propeller

## References


[1] Weitendorf, E. A., 1989, ''25 Years Research on Propeller Excited Pressure Fluctuations and Cavitation,'' *Proc. ASME Int. Symp. On Cavitation Noise and Erosion in Fluid Systems*, ASME, New York, **FED-18**, pp. 1–10.

[2] Duttweiler, M. E., and Brennen, C. E., 2002, ''Surge Instability on a Cavitating Propeller,'' J. Fluid Mech., **458**, pp. 133–152.

[3] Brennen, C. E., 1994, *Hydrodynamics of Pumps*, Oxford University Press and Concept ETI, New York.

[4] Brennen, C. E., and Acosta, A. J., 1973, ''Theoretical, Quasi-Static Analyses of Cavitation Compliance in Turbopumps,'' J. Spacecr. Rockets, **10**(3), pp. 175–180.

[5] Brennen, C. E., 1978, ''Bubbly Flow Model for the Dynamic Characteristics of Cavitating Pumps,'' J. Fluid Mech., **89**, pp. 223–240.

[6] Tsujimoto, Y., Kamijo, K., and Yoshida, Y., 1993, ''A Theoretical Analysis of Rotating Cavitation in Inducers,'' ASME J. Fluids Eng., **115**, pp. 135–141.

[7] Tulin, M. P., 1953, ''Steady, Two-Dimensional Cavity Flows About Slender Bodies,'' Tech. Report 834, David Taylor Model Basin.

[8] Brennen, C. E., 1995, *Cavitation and Bubble Dynamics*, Oxford University Press, New York.

[9] Otsuka, S., Tsujimoto, Y., Kamijo, K., and Furuya, O., 1996, ''Frequency Dependence of Mass Flow Gain Factor and Cavitation Compliance of Cavitating Inducers,'' ASME J. Fluids Eng., **118**, pp. 400–408.

[10] Watanabe, S., Tsujimoto, Y., Kamijo, K., and Furuya, O., 1998, ''An Analysis of Cavitation Characteristics by Singularity Method,'' Trans. Jpn. Soc. Mech. Eng., Ser. B, **64**(621), pp. 1285–1292 (in Japanese).

[11] Watanabe, S., Sato, K., Tsujimoto, Y., and Kamijo, K., 1999, ''Analysis of Rotating Cavitation in a Finite Pitch Cascade Using a Closed Cavity Model,'' ASME J. Fluids Eng., **121**(4), pp. 834–840.